Instability of a vertical chemical front: Effect of viscosity and density varying with concentration

Subramanian Swernath and S. Pushpavanam[a)]
Department of Chemical Engineering, I. I. T. Madras, Chennai, Tamilnadu 600036, India

(Received 24 June 2007; accepted 6 December 2007; published online 14 January 2008)

In this work we analyze the behavior of a chemical front in a vertical porous medium. A homogeneous autocatalytic reaction occurs in the liquid phase. The column is filled with a chemical species and the reaction is initiated at one end of the vertical column by instantaneously adding the product. The reaction occurs at the interface of the products and the reactants. This causes the reaction front to move down (up) when the product is added to the top (bottom). The front or interface demarcates the domain into two regions: one rich in the reactants and the other rich in products. In this work chemohydrodynamic instabilities are studied, when the density and viscosity of the reactants and products are different and concentration dependent. The dependency of these properties on concentration is explicitly considered. We assume the process to be isothermal and other properties such as diffusivity and permeability to be constant. A traveling wave of chemical concentration is generated in the upward direction (when the products are introduced at the bottom) as the product reacts at the interface. The stability of the interface is determined by the viscosity and density of the two fluids. A shooting method in combination with a Runge–Kutta fourth-order scheme is used for generating the base state of the traveling front. Here, the conditions at which an interfacial instability induced by the density gradients is stabilized due to the viscosity dependence on concentration are determined. Linear stability predictions are determined by inducing perturbations on the traveling wave base state and analyzing their evolution. The effect of various parameters on the stability of the flow was calculated and compared with the nonlinear simulations. The nonlinear problem is modeled using the stream-function, vorticity equations. These equations are solved using a second-order finite difference scheme in space and first-order forward difference scheme in time. The instability predicted from the linear stability analysis is validated with nonlinear simulations. © *2008 American Institute of Physics*. [DOI: 10.1063/1.2829081]

I. INTRODUCTION

Hydrodynamic fingering instabilities in porous media have been investigated extensively in the past few decades. The interaction between reaction and diffusion can result in a chemical reaction front moving as a traveling wave with no bulk motion of the liquid phase. The wave velocity is determined by the interaction of autocatalytic chemical kinetics and diffusion. In this state, the interface between the reactant rich region and the product rich region remains sharp and flat. In the presence of density gradients, the interface can become unstable. In this unstable state there is bulk motion in the liquid phase and the interface exhibits fingerlike structures. The system now exhibits spatial patterns. Numerous experimental as well as theoretical investigations have been carried out to analyze this phenomenon. The spatiotemporal dynamics results from the interplay between the autocatalytic chemical reaction and hydrodynamics. Consider a case when there are density changes moving across the reaction-diffusion front in the direction of gravity. This can induce a Rayleigh–Taylor instability if the heavier fluid is placed on top of the lighter fluid. Miscible systems with chemical reactions are prone to density driven instabilities in such a buoyantly unstable situation.

The experimental observation of channeling in a sugar sweetening process triggered significant research in the area of hydrodynamic instabilities in a porous media.[1] The initial stages of research focused on horizontal flows where the density effect was not significant. The instability here is generated by the viscosity changes. Nonlinear simulations of these systems were carried out using a finite difference technique[2,3] to understand the long term dynamics. Tan and Homsy[4] used efficient algorithms based on spectral methods for these simulations. Further, they simulated the system using a ψ-ω formulation instead of the pressure-velocity formulation, as was used by the earlier researchers. The predictions were compared with the linear stability analysis of Tan and Homsy[5] at the initial stages. The basics of the fingering phenomena and a detailed review of the contrasts and the similarities of miscible and immiscible flows is described by Homsy.[6] Reactive instabilities have been studied in a horizontal domain with a bistable (cubic) kinetics by De Wit and Homsy,[7,8] where they observe drop formation. These instabilities stem from the viscosity differences as the fluid moves; they arise in horizontal flows and are called viscous fingering. The viscous fingering is triggered only in the presence of a definite injection velocity.

In contrast to this, several studies have been carried out in density fingering which we now discuss. Here, the chemi-

a)Electronic mail: spush@iitm.ac.in.

cal front propagates in the vertical direction with no bulk motion of the fluid. Several experimental investigations have been carried out on the density fingering in an iodate-arsenous acid (IAA) system.[9] Deceleration of some fingers resulting in the acceleration of their neighbors has been observed while doing a temporal evolution study.[10] Experimental predictions of spatial modes of instability was done and was compared with two-dimensional (2-D) Stokes simulations.[11] Upward propagating fronts were studied and the experimental results were compared with the linear stability analysis predictions.[12]

Theoretical studies in density fingering include isothermal as well as nonisothermal reactions. The effect of kinetic parameters on the onset of convection has been analyzed theoretically.[13] Linear stability analysis has been carried out using the full three-dimensional (3-D) Stokes equations[14] as well as using Darcy's law.[15,16] The front propagation was compared for both convective and convectionless fronts. Convective fronts were found to move faster with respect to a convectionless front.[17] Two-dimensional linear stability analysis was carried out and the results were compared with 3-D lattice Bhatnagar–Gross–Krook simulations.[18] Tracking the interface and its characteristics have been carried out using a free boundary problem formulation. The tangent angle and the perimeter of the front have been used as the analysis variables.[19] Nonisothermal effects along with the concentration effects on density have been studied in a laterally unbounded system. Linear stability analysis was carried out for this system.[20] The IAA system admits two steady states. In the absence of convection we have traveling front from the unstable steady state to the stable steady state.[21] The reaction term is represented using a compact kinetic expression that allows chemical fronts between two steady states. A one variable model representing the evolution of iodide concentration was found to be sufficient to describe the reaction an capable of producing fingering instabilities.[22] This work also discusses the generation of the sharp front which travels at a speed governed by diffusion if the hydrodynamic effects are absent. This cubic one variable kinetics representative of iodate-arsenous acid reaction is valid only for the case when arsenous acid is in excess. Some other reactions such as chlorite-tetrathionate (CT) [23] and polymerization have been studied theoretically[24] and experimentally.[25] Experimental studies were carried out to study the factors affecting front shape, velocity, conversion, etc.[25] They observed different spin modes by varying the heat loss, initiator concentration, etc. In Ref. 24, they discuss the polymerization propagation fronts. The main focus of that work is on the experimental and theoretical study of the effect of convection on both upward and downward moving polymerization fronts. The viscosity variations were significant for the reactions they had considered. In polymerization reactions researchers have observed reactions propagating due to the thermal effects.[26] A theoretical study of thermal wave propagation in which chemical conversion occurs has been studied.[27] They in turn determined analytically the structure of the wave, propagation velocity, amount of conversion, etc. Heat effects due to the reaction have been incorporated in some recent papers for IAA and CT reactions also.[28–30] Analysis using nonlinear simulations in a vertical flow was done by De Wit[31] for the IAA kinetics with the viscosity of the solution assumed to be a constant. Drop formation was observed in the vertical geometry also by De Wit *et al.*[32] This was attributed to the form of kinetics which admitted two stable steady states. The Boussinesq approximation has been used in all the literature cited where the effect of density variation is considered only in the gravitational term. Pure density fingering was also discussed experimentally[33] and theoretically.[34] The simulations were carried out in Ref. 34 using the Stokes regime and here the dispersion curves varied as a function of time. In all the above studies viscosity was always assumed to be a constant in the vertical alignment. In this work we incorporate the viscosity dependency on concentration and seek the conditions under which it can stabilize a density unstable configuration. Such systems are important in the area of polymerization where viscosity changes significantly as the reaction occurs. The motivation for this study is to determine the conditions when viscosity changes can stabilize or amplify the instability in an unstable interface. There is no injection velocity in the density driven situation. Hence, viscous fingering is absent as the driving force required to generate the phenomenon will not come into the picture.

In Sec. II, we formulate the model of the system and recast the governing equations into their nondimensional counterparts. The viscosity and density are assumed to be functions of concentration. Diffusivity and permeability are assumed constant. In Sec. III, we generate the base state of the solution in the form of a traveling front. This shows a sharp change in concentration across the front. The effect of Da on the traveling front is analyzed. The next section discusses the linear stability of the wave. An infinitesimal disturbance is incorporated and the evolution of the disturbance is studied. The results are depicted as dispersion curves. Section V discusses the results obtained from nonlinear simulations. The predictions of the linear stability are validated with the nonlinear simulations. These simulations confirm that the linearly unstable system exhibit a fingered interface.

II. MODEL

We consider a 2-D porous media filled with a reactant as shown in Fig. 1. The gravity field is aligned along the positive x direction as shown in the figure. The product species of concentration c_1^* is introduced at the bottom and thus invades the reactants lying in the upper portion of the porous medium. The reaction occurs only at the interface separating the two fluids since it is autocatalytic in nature and requires both reactants and products to progress. The interface of the system starts moving upwards as a traveling front with a constant velocity as time progresses. The stability of this interface separating the two fluids depends on the density of the two fluids. If the reactants are lighter than the products then we have a planar front. If the reactants are heavier than the products the system is unstable and the interface gets deformed in the presence of the slightest perturbation. The latter condition leads to the formation of fingered structures in the medium. These arise due to the classical Rayleigh–Taylor instability. This study focusses on theoretically ana-

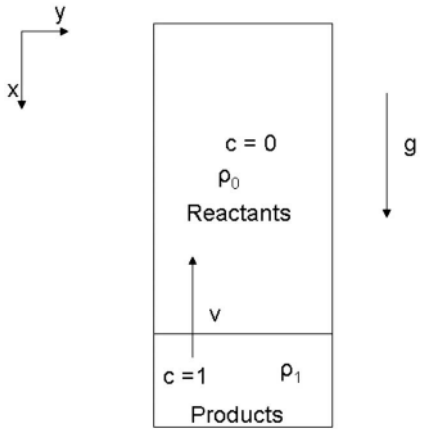

FIG. 1. Schematic model of the system under investigation.

lyzing the system behavior when both fluid density and viscosity vary with concentration. The system is governed by the continuity equation and the momentum equation in the form of Darcy's law. The transport of chemical species is represented by the convective-diffusion equation. We use the Boussinesq approximation where we include the effect of density dependence on concentration only in the gravity term of the momentum equation.

The equations which govern the fluid flow and the ones which represent the interactions between hydrodynamics and chemical reactions are now described.

The equation of continuity is

$$\nabla^* \cdot \vec{u}^* = 0. \tag{1}$$

For laminar flow, Darcy's law, which determines the pressure drop in a porous medium or a Hele-Shaw cell, can be written as

$$\nabla^* P^* = -\frac{\mu^*}{K}\vec{u}^* + \rho^* g \vec{i}_x. \tag{2}$$

A convective-diffusion equation is used to describe the species transport and is given by

$$\frac{\partial c^*}{\partial t^*} + \vec{\mathbf{u}}^* \cdot \nabla^* c^* = D\nabla^{*2} c^* - k_r c^* (c^* - c_1^*)(c^* + d^*). \tag{3}$$

Here, c^* represents concentration of the product species. Similarly, ∇^* represents gradient x^*, y^* as independent variables. In this work the density and viscosity are both assumed to be dependent on concentration $\rho^* = \rho(c^*)$ and $\mu^* = \mu(c^*)$. The other physical parameters such as permeability (K) and diffusion coefficient (D) are, however, assumed to be constant. The density is assumed to vary linearly with product concentration and the viscosity variation with the product concentration is taken to be exponential. The functional forms of these relationships are given below:

$$\rho^*(c^*) = \rho_1^* + (\rho_0^* - \rho_1^*)\left[1 - \frac{c^*}{c_1^*}\right],$$
$$\mu^* = \mu_0^* e^{-Rc^*}. \tag{4}$$

A characteristic velocity U is defined such that it balances the viscous and buoyancy forces. This yields $U = \Delta\rho^* gK/\nu*$, where $\nu^* = \mu^*/\rho_0^*$ and $\Delta\rho^* = (\rho_0^* - \rho_1^*)/\rho_o^*$.

The characteristic length and time scales are chosen as $L_{\mathrm{ch}} = D/U$ and $\tau_H = D/U^2$, respectively.

The aspect ratio represented by A is defined as $A = L_x/L_y$. The dimensionless parameter Ra is defined as $\Delta\rho^* L_y^* Kg/\nu^* D$. This represents a measure of the dimensionless width of the domain. The governing variables are nondimensionalized using these scales. The corresponding dimensionless variables are

$$x = \frac{x^*}{L_{\mathrm{ch}}}, \quad y = \frac{y^*}{L_{\mathrm{ch}}}, \quad u = \frac{u^*}{U}, \quad t = \frac{t^*}{\tau_H},$$
$$P = \frac{P_1^* K}{\mu_0^* D}, \quad \rho = \frac{\rho^*}{\rho_0^*}, \quad c = \frac{c^*}{c_1^*}, \quad d = \frac{d^*}{c_1^*}.$$

This scaling is implemented whenever $\rho_0 > \rho_1$. The domain in the x direction varies from 0 to A Ra and in the y direction from 0 to Ra in the nondimensional representation. The governing equations after converting to their nondimensional form are recast as

$$\nabla \cdot \vec{u} = 0. \tag{5}$$

The momentum balance is of the form

$$\nabla P = -\frac{\mu}{K}\vec{u} + (1 - c)\vec{i}_x, \tag{6}$$

where $\mu = \mu^*/\mu_0$.

The species transport is given by

$$\frac{\partial c}{\partial t} + \vec{u} \cdot \nabla c = \nabla^2 c - \mathrm{Da}\, c(c-1)(c+d), \tag{7}$$

where $\mathrm{Da} = Dk_r c_1^{*2}/U^2$ represents the ratio of dispersive time scale to the reactive time scale. Da is called the Damköhler number. The equations are converted to streamfunction-vorticity or ψ-ω form using $u = \partial\psi/\partial y$ and $w = -\partial\psi/\partial x$. The dimensionless equations in the streamfunction-vorticity formulation that describe the system are

$$\nabla^2 \psi = R\left[\frac{\partial\psi}{\partial x}\frac{\partial c}{\partial x} + \frac{\partial\psi}{\partial y}\frac{\partial c}{\partial y}\right] + \frac{1}{e^{-Rc}}\frac{\partial c}{\partial y}, \tag{8}$$

$$\frac{\partial c}{\partial t} + \frac{\partial\psi}{\partial y}\frac{\partial c}{\partial x} - \frac{\partial\psi}{\partial x}\frac{\partial c}{\partial y} = \nabla^2 c - \mathrm{Da}\, c(c-1)(c+d). \tag{9}$$

The system of Eqs. (8) and (9) are solved subject to initial and boundary conditions. The right-hand side of Eq. (8) represents the $-\omega$ term. We need both these conditions for concentration. For the streamfunction, we need only boundary conditions. No conditions are required for the vorticity function as it is governed by an algebraic equation. For dynamic simulations, the domain in the x direction is divided into

three parts: $(0, L^*_{i-1})$, L^*_i, and $(L^*_{i+1}, A\,\mathrm{Ra})$. Here, L^*_i represents the x distance of the ith grid point from the top. The initial conditions at $t=0$ used for the simulations are

$$0 < x < L^*_{i-1}, \quad c = 0,$$
$$L^*_{i+1} < x < A\,\mathrm{Ra}, \quad c = 1. \tag{10}$$

Along $x=L^*_i$, we specify a random number in the range (0,1) which specifies the disturbance in the system. The random number generates the disturbance in the concentration. The evolution of concentration as time progresses is studied by numerically simulating the governing equations.

Along the boundaries $x=0$ and $x=A$ Ra, we use Dirichlet boundary conditions for concentration. We impose $\psi=0$ along the boundaries $x=0$ and $x=A$ Ra. Periodic boundary conditions are applied along the y direction for both c and ψ. These can be represented mathematically as

$$c(x=0)=0, \quad c(x=A\,\mathrm{Ra})=1,$$
$$c(y=0)=c(y=\mathrm{Ra}), \quad \left.\frac{dc}{dy}\right|_{y=0} = \left.\frac{dc}{dy}\right|_{y=\mathrm{Ra}}, \tag{11}$$

$$\psi(x=0)=0, \quad \psi(x=A\,\mathrm{Ra})=0,$$
$$\psi(y=0)=\psi(y=\mathrm{Ra}), \quad \left.\frac{d\psi}{dy}\right|_{y=0} = \left.\frac{d\psi}{dy}\right|_{y=\mathrm{Ra}}. \tag{12}$$

Typical values of various parameters that have been reported by experimentalists for IAA reactions are $\rho_0=1.002$ g/cm^3, $\nu=0.0099$ cm^2/s, $\Delta\rho=1.3\times10^{-4}$, Da=1.71, and $d=0.0021$. Similarly, in polymerization processes,[24] the typical values of various parameters are Ra=50, Prandtl number=10, and adiabatic temperature change=140. We observe that even a small difference in density is sufficient to trigger the hydrodynamic instability.

III. TRAVELING FRONTS

The system of Eqs. (5)–(7) admits a solution in the form of a traveling wave. The traveling front occurs in the absence of any convection or bulk motion and is induced primarily by the interaction of the autocatalytic chemical kinetics and diffusion in the system. This wave is one dimensional and is a chemical concentration wave. Equation (7) in the absence of convection admits two spatially uniform steady states: $c=1$ is a stable chemical steady state corresponding to the products and $c=0$ is the unstable steady state corresponding to the reactants.[30] The concentration wave is dependent on a single independent variable z given by $z=x+vt$, where v is the traveling front velocity. The spatial and temporal variation of concentration in this traveling wave can be written as $c(x,t)=1/1+e^{-\sqrt{\mathrm{Da}/2}(x+vt)}$ in a spatially unbounded domain. The velocity v of the traveling wave is given by $v=\sqrt{\mathrm{Da}/2}(1+2d)$.[16] This represents physically the rate of movement of the interface in the upward direction due to the reaction at the interface. The governing equation which generates the traveling wave is obtained from Eqs. (5)–(7), assuming concentration is a function of only z. The traveling wave form is the solution of

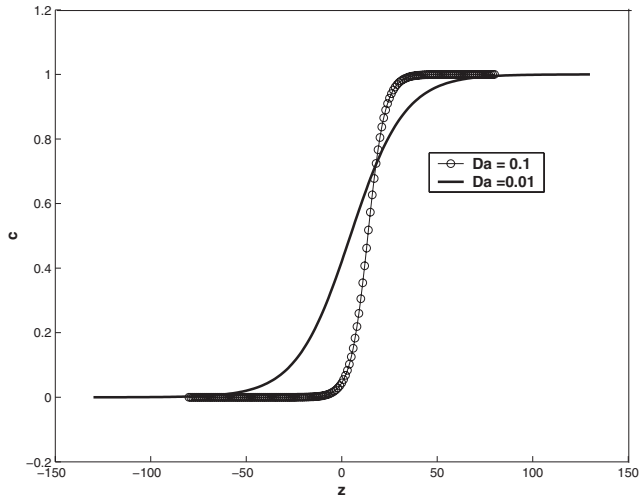

FIG. 2. Effect of Da on the traveling wave front.

$$v\frac{dc_{ss}}{dz} = \frac{d^2c_{ss}}{dz^2} + \mathrm{Da}\,f(c_{ss}), \tag{13}$$

where $f(c)=-c(c-1)(c+d)$. The traveling wave solution of Eq. (13) for a finite domain is obtained by numerically solving Eq. (13) subject to suitable boundary conditions. Instead of the boundary conditions $c(-\infty)=0$ and $c(\infty)=1$ for the infinite domain, the conditions were chosen as $c(-z_1)=0$ and $c(z_1)=1$. The domain $(-z_1, z_1)$ was varied by changing z_1 to ensure the domain independence of the solution. The second-order differential equation (13) is converted to two first-order ordinary differential equations and is solved as a boundary value problem. A shooting method in combination with the Runge–Kutta (fourth-order) method was used for numerically determining the traveling wave solution governed by Eq. (13).

The traveling wave concentration and the gradient $c_{ss}=c_{ss}(z)$, $dc_{ss}(z)/dz$ are obtained directly at all the grid points in this method. The traveling front obtained numerically for finite domains is shown in Fig. 2 for Da=0.01 and Da=0.1 for $d=0.1$. The grid spacing used for the simulations is 1, but they were validated with other spacings of 0.5 and 2 to ensure grid space independence. The range of the domain to obtain a converged solution varied with Da. It was −135 to +135 for Da=0.01. This range was lower for a higher Da, as the wave front becomes sharp as we increase Da. The velocity of the wave increases and the total length of the domain required for the traveling wave to become domain independent reduced with an increase in Da. Figure 3 depicts the variation of viscosity, density and concentration as a function of z (traveling wave coordinate) for Da=0.01. The density variation is very low, of the order of 10^{-3}, and hence it is plotted on a separate scale on the right side.

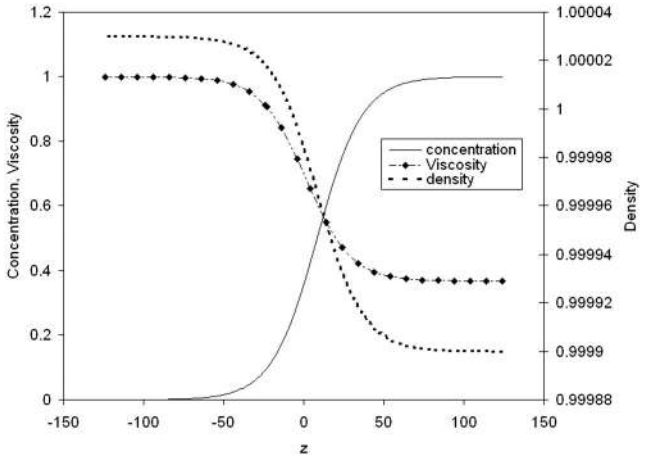

FIG. 3. Effect of ρ, μ, c as a function of z (traveling wave coordinate).

IV. LINEAR STABILITY

The stability of the traveling wave obtained was determined to analyze the system behavior. A stable behavior implies that the concentration does not vary across the cross section and the concentration front moves as a planar front with a constant velocity. Linear stability analysis is used in our case for predicting the onset of stability. Instability is characterized by the interface (the surface separating the $c=0$ and $c=1$ regions) deforming as fingers and accompanied by the onset of convection. A spatial perturbation is given to the variables and its evolution is studied. The base state is the traveling wave obtained numerically in the previous section for a finite domain. This base state corresponds to

$$u_{ss}=0, \quad w_{ss}=0, \quad c_{ss}=c_{ss}(z), \quad \text{and } p_{ss}=p_{ss}(z).$$

We analyze the deviation of the variables from this base state. These are defined as

$$\begin{aligned}\tilde{c}&=c-c_{ss},\\ \tilde{u}&=u-u_{ss},\\ \tilde{w}&=w-w_{ss},\\ \tilde{P}&=P-P_{ss}.\end{aligned} \tag{14}$$

The viscosity variation with concentration is linearized as

$$\mu=\mu_{ss}+\left.\frac{d\mu}{dc}\right|_{ss}\tilde{c}. \tag{15}$$

Substituting Eqs. (14) in Eqs. (5)–(7) and subtracting the base state values, we obtain the system of equations that describe how the perturbations evolve with time and space:

$$\frac{\partial\tilde{u}}{\partial z}+\frac{\partial\tilde{w}}{\partial y}=0, \tag{16}$$

$$\frac{\partial\tilde{P}}{\partial z}=-\mu_{ss}\tilde{u}-\tilde{c}, \tag{17a}$$

$$\frac{\partial\tilde{P}}{\partial y}=-\mu_{ss}\tilde{w}, \tag{17b}$$

$$\frac{\partial\tilde{c}}{\partial t}+v\frac{\partial\tilde{c}}{\partial z}+\tilde{u}\frac{\partial c_{ss}}{\partial z}=\frac{\partial^2\tilde{c}}{\partial z^2}+\frac{\partial^2\tilde{c}}{\partial y^2}-\mathrm{Da}\left.\frac{\partial f}{\partial c}\right|_{ss}\tilde{c}. \tag{18}$$

We seek solutions for Eqs. (16)–(18) in the form of normal modes; i.e., with a periodic dependency in the y direction. The deviation of the variables is taken to be of the form

$$\begin{aligned}\tilde{c}(z,y,t)&=\bar{c}(z)e^{\sigma t}e^{iky},\\ \tilde{u}(z,y,t)&=\bar{u}(z)e^{\sigma t}e^{iky},\\ \tilde{w}(z,y,t)&=\bar{w}(z)e^{\sigma t}e^{iky},\\ \tilde{P}(z,y,t)&=\bar{P}(z)e^{\sigma t}e^{iky},\end{aligned} \tag{19}$$

with σ representing the growth rate of the disturbances and k representing the wave number. We eliminate $\bar{w}$ and $\bar{P}$ from Eqs. (16)–(18) and obtain the final set of ordinary differential equations that determine the linear stability as

$$\frac{d^2\bar{u}}{dz^2}+\frac{1}{\mu_{ss}}\frac{d\mu_{ss}}{dz}\frac{d\bar{u}}{dz}-k^2\bar{u}-\frac{k^2}{\mu_{ss}}\bar{c}=0, \tag{20}$$

$$\frac{d^2\bar{c}}{dz^2}-k^2\bar{c}-v\frac{d\bar{c}}{dz}-\bar{u}\frac{dc_{ss}}{dz}-\mathrm{Da}\frac{\partial f}{\partial c}\bar{c}=\sigma\bar{c}. \tag{21}$$

Equations (20) and (21) are discretized using a second-order central finite difference. These are written for each individual node. This results in $2m$ equations for a total of m nodes in the x direction. The equations can be expressed in the general matrix form as

$$(A)\begin{pmatrix}\bar{u}\\ \bar{c}\end{pmatrix}=\sigma\begin{pmatrix}0 & 0\\ 0 & 1\end{pmatrix}\begin{pmatrix}\bar{u}\\ \bar{c}\end{pmatrix}. \tag{22}$$

Equation (22) represents a generalized eigenvalue problem that can be written mathematically as $Ax=\sigma Bx$. The largest eigenvalue σ of the matrix A is obtained for various wave numbers k. When this is negative the system is stable since all the other eigenvalues are also negative. The numerical code used for obtaining the maximum eigenvalue is developed in MATLAB®. The dependency of the growth constant, i.e., the largest eigenvalue of A on k, is depicted as dispersion curves.

Figure 4 shows the dispersion curves for two situations for the parameters Da=0.01, $d=0.1$, and $R=0$. The first situation consists of heavier products introduced at the bottom of the chamber filled with lighter reactants. Here, the heavier products lie below the lighter reactants resulting in a gravitationally (density) stable situation. The dispersion curve lies entirely below the x axis with the maximum eigenvalue always being negative. This is depicted as a line with circles in Fig. 4. In the second case, we have the chamber filled with reactants, and the products which are lighter than the reactants are introduced at the bottom. Here, the system shows density induced instability and the dispersion curve (depicted as solid line) has a maxima above the z axis. This results in

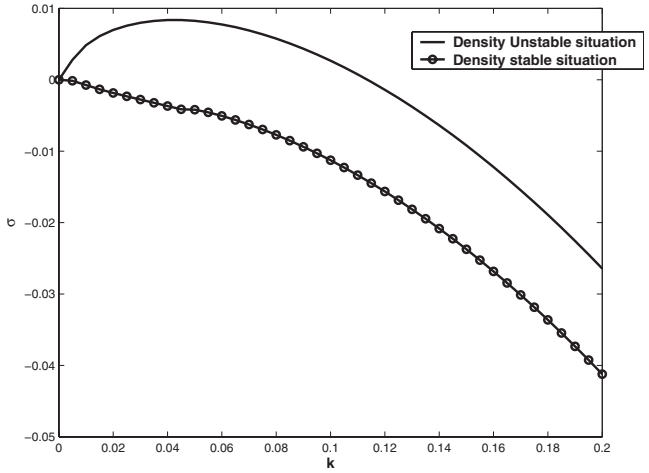

FIG. 4. Density stable and unstable reaction fronts for Da=0.01, $R=0$, and $d=0.1$. Line with circles represents stable and "—" represents unstable.

an unstable flow where we see fingering patterns. The maximum of the growth constant σ occurs for $k=0.043$, and this wave number determines the reciprocal of the wavelength of the spatial pattern observed when instability is initiated. The numerical calculation of the unstable and stable dispersion curves is carried out by means of changing the term $-k^2/\mu_{ss}\bar{c}$ to $+k^2/\mu_{ss}\bar{c}$ in Eq. (20). This term arises due to the gravity part in the x component of Darcy's law. This occurs because in the density unstable situation $\rho_0>\rho_1$ and both Ra and U are positive, as defined in the paragraph after Eq. (4). For the density stable situation, we need to define $\Delta\rho$ as $(\rho_1-\rho_0)/\rho_0$, so as to keep U and Ra positive. Figure 5(a) shows the effect of Da and R on the dispersion curve when a heavy reactant solution lies above the lighter product solution $(\rho_0>\rho_1)$. Here, the system shows a density induced instability. The interface of the traveling front moves upward at a velocity dependent on Da and d. An increase in Da for a fixed R results in an increase in the growth rate and the dispersion curve is shifted upwards. An increase in Da physically implies that the reaction rate dominates diffusion and convection. A large value of Da decreases the stabilization effect caused by diffusion. The traveling wave becomes sharp with an increase in Da. The wavelength of the fingers is reduced with an increase in Da as the maxima of the dispersion curve moves to the right. The results for the constant viscosity fluid $(R=0)$ were reproduced for the same set of parameters as was used by De Wit.[16] The effect of the parameter Da on the dispersion curve is similar to the trends already observed by other researchers.[16] There, the viscosity was taken to be constant and the density was assumed to vary linearly with concentration. In the present work we use the same functional representation for density, but viscosity is assumed to depend on the concentration of the products through an exponential relationship. The incorporation of the viscosity dependency on concentration does not affect the chemical kinetics. Consequently the effect of Da and d on the dispersion curves are similar to that observed previously.[16] Figure 5(a) also depicts the effect of parameter R on the stability of the system. It is seen that as R increases from 0 to 1, the system becomes more unstable. $R>0$ implies that the front moves from low viscosity to high viscosity region.

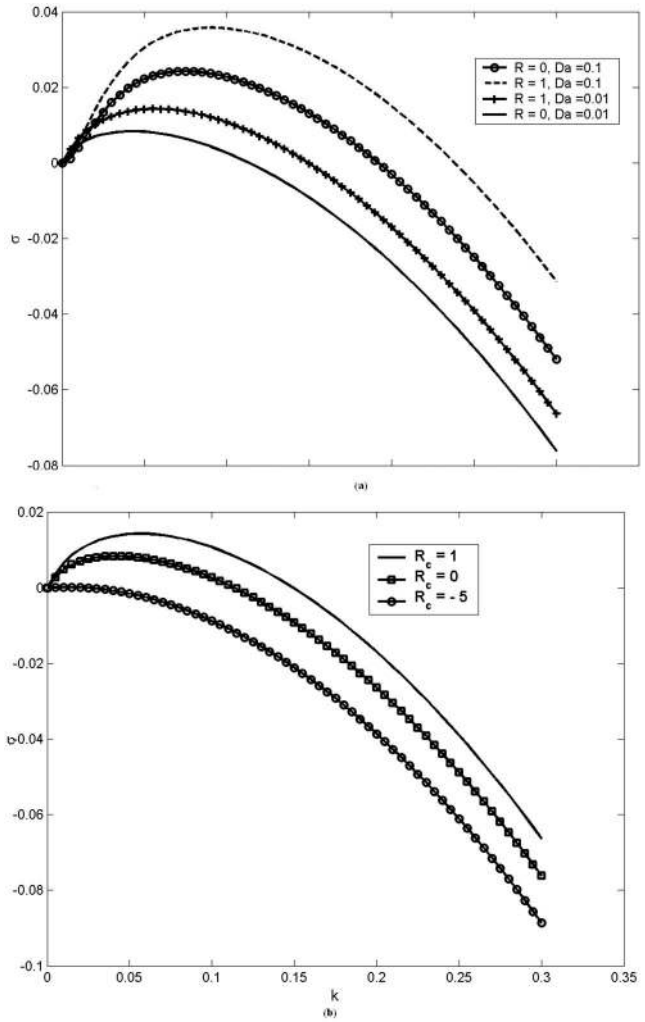

FIG. 5. Dispersion curve showing the variation of growth constant on wave number. (a) Effect of Da for $R=0$ and $R=1$. (b) Effect of R.

Figure 5(b) shows how the stability of the interface depends on the mobility ratio R for Da=0.01 and $d=0.1$. The results are for a gravitationally unstable situation where the lighter products invade the heavier reactants from the bottom. The interface keeps moving upward and exhibits fingering when the viscosity is independent of concentration; i.e., when $R=0$. When $R=1$, the viscosity of the products is lower than that of the reactant. Consequently, the lower viscous fluid invades the higher viscous fluid and this serves to make the system more unstable. The dispersion curve shifts upwards for $R>0$. For $R<0$, the curve starts shifting downward and we observe that for $R=-5$, the dispersion curve is completely below the x axis. Here, the increase in viscosity of the products stabilizes the density unstable system entirely. The hydrodynamics is strongly affected here by the introduction of viscosity dependency on concentration and this is seen in the shift of the dispersion curves with the parameter R.

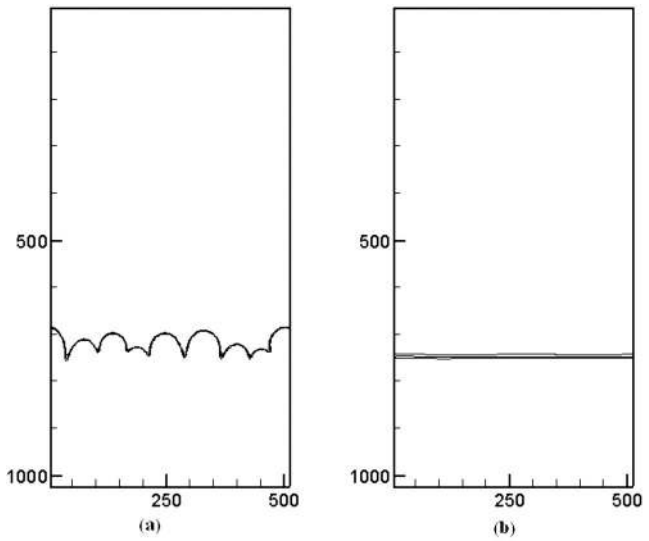

FIG. 6. Nonlinear simulation showing the variation of growth constant on wave number. (a) Density unstable flow and (b) density stable flow.

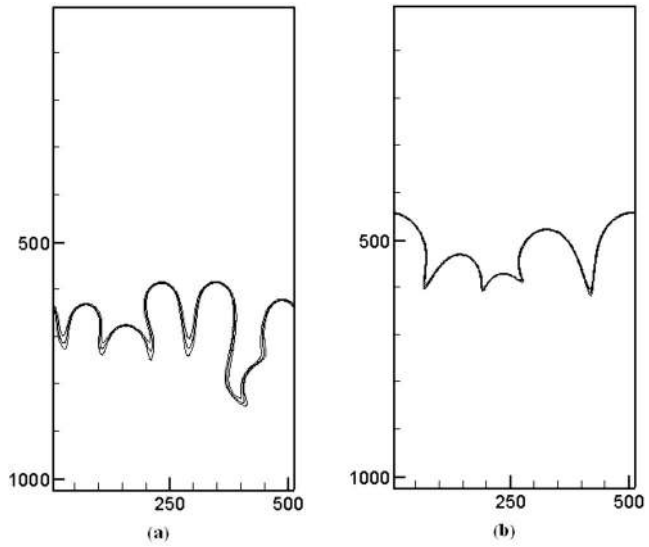

FIG. 8. Nonlinear simulation results showing the concentration contours (0.1–0.3) illustrating the effect of Da for $R=1$, $d=0.1$, $t=500$ s, Ra=512. (a) Da=0.01 and (b) Da=0.1.

V. NONLINEAR SIMULATION

To verify the predictions of the linear stability analysis, we have also simulated the nonlinear system dynamically. A finite difference scheme was used for the simulation of Eqs. (8) and (9). All the simulations are carried out for Ra=512 and $A=2$ unless otherwise mentioned. The grid size chosen is 256×128 with 256 rows along the vertical direction (x direction) and 128 along the y direction. This results in a uniform grid spacing of four units in both the directions. This grid spacing was arrived at after a grid independence study was carried out.

The equations are solved using a second-order central finite differencing scheme in space. The discretization used is Forward in Time Central in Space (FTCS). Nonlinear simulations are used to predict the long term dynamics. The various steps in the numerical algorithm for the simulation of Eqs. (8) and (9) are outlined below.

(1) Equation (9) is integrated numerically to calculate $c(t+\Delta t)$ at each and every grid point using the values of $\psi(t)$ and $c(t)$ at the earlier time instant.

(2) The known $\psi(t)$ and $c(t+\Delta t)$ are used for evaluating the terms occurring on the right-hand side of Eq. (8) and the Laplacian of $\psi(t+\Delta t)$ is determined on the left-hand side. The variable $\psi(t+\Delta t)$ is iterated using a point-by-point scheme until the convergence of ψ is assured.

(3) $c(t+\Delta t)$ is recalculated in Eq. (9) using the estimated value of $\psi(t+\Delta t)$.

(4) These steps are repeated until we have convergence of c and ψ for the time step.

(5) We then proceed to the next time step.

The nonlinear dynamics of the fluid interface is analyzed by simulating the system for several combinations of parameters. The initial stages of the interfacial dynamics obtained are compared with the linear stability predictions. Figures 6(a) and 6(b) show the nonlinear simulation prediction for the cases where the heavier liquid is at the top and bottom, respectively. Figure 6(a) depicts the arrangement where the system shows instability. Here, the lighter product solution

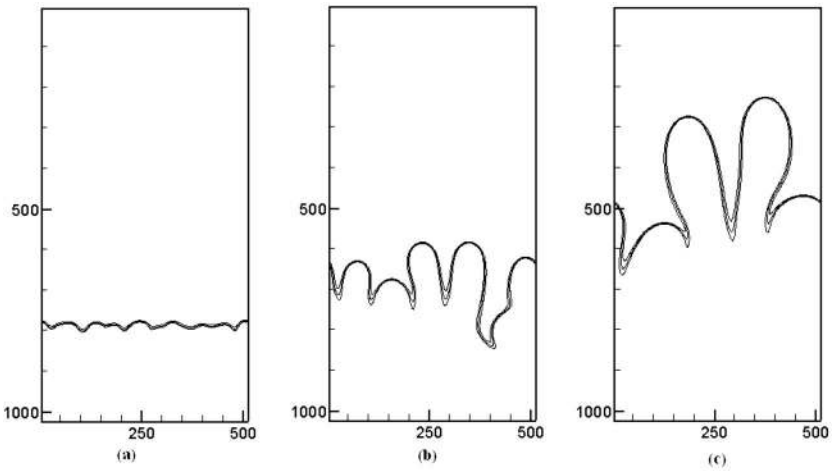

FIG. 7. Nonlinear simulation results showing the time evolution of concentration contours (0.1–0.3) for unstable displacement for $R=1$, Da=0.01, $d=0.1$, Ra=512. (a) Time=100 s, (b) time=500 s, and (c) time=1200 s.

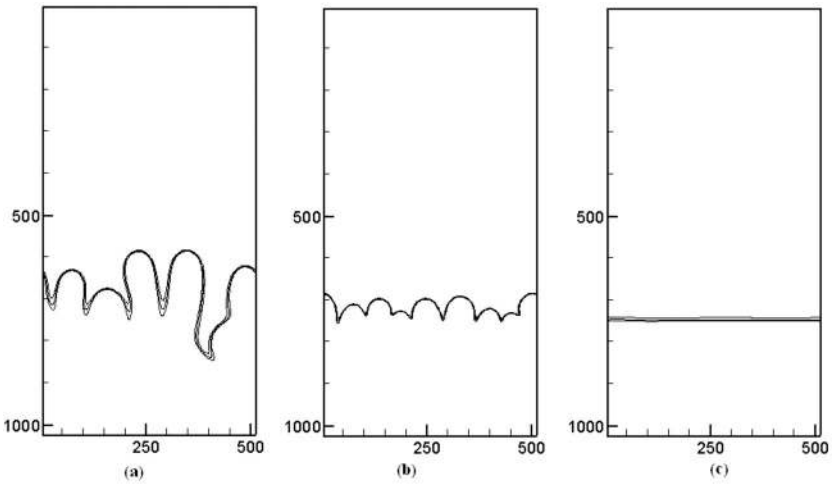

FIG. 9. Nonlinear simulation results showing the concentration contours (0.1–0.3) for the effect of viscosity on density instability when lighter products are injected at the bottom for Ra=512, Da=0.01, d=0.1, t=300 s. (a) R=1, (b) R=0, and (c) R=−5.

from the bottom invades the heavier reactant solution at the top resulting in a fingered interface. When the heavier solution lies below the lighter solution, the system shows a stable planar interface represented by Fig. 6(b). This situation corresponds to a heavier product solution invading the lighter reactant solution on top. These nonlinear simulation predictions are in agreement with the results of the linear stability analysis of Fig. 4. The effect of viscosity dependence on concentration was neglected in these simulations; i.e., we take R=0. The time evolution of the stable front shows that it always remains stable. Figures 7(a)–7(c) show the time evolution profiles when both density and viscosity have a destabilization effect (R=1). For low times (t=100 s) the interface is not deformed significantly, but at a later time instant (t=500 s) distinct fingers are visible. This is in contrast to Fig. 6(b), where the interface or reaction front keeps moving as a stable planar front at extremely large time instants also. As we evolve in time, when the system is unstable the fingers merge and the number of fingers gets reduced; at large times, just three fingers are obtained [Fig. 7(c)]. For even larger times, these merge to yield a single dominant finger. This is a characteristic of the nonlinear dynamics at large times, which leads to the decrease in the number of fingers as time evolves.

Figures 8(a) and 8(b) discuss the effect of Da on the interface shape for R=1, d=0.1 at a time instant of 500 s. An increase in Da leads to faster moving fronts. Here, as the velocity of the traveling wave is proportional to $\sqrt{\text{Da}}$, the average interface position has moved further upwards for the higher Da for the same time instant. The nonlinear simulations confirm the critical wave number predictions of the linearized stability analysis at early time instants. Instability is predicted by the linear stability analysis for these parameters [see Fig. 5(a)] and these have been confirmed by the nonlinear simulations.

Figures 9(a)–9(c) depict the concentration contours for a gravitationally unstable situation. Here, the lighter liquid is placed below a heavier one and hence the effects of gravity tend to destabilize the interface. Figure 9(a) shows the fingering trends when $R>0$. Here, the lighter fluid is less viscous than the heavier more viscous fluid. Figure 9(b) shows the chemically driven density fingering. Here, no viscosity gradient is present. Figure 9(c) shows how the viscosity dependence on concentration ($R<0$) can stabilize an interface, which is gravitationally unstable. The stabilization of the front is achieved by a large negative R. This continues to be stable with progress in time. In the case of an unstable inter-

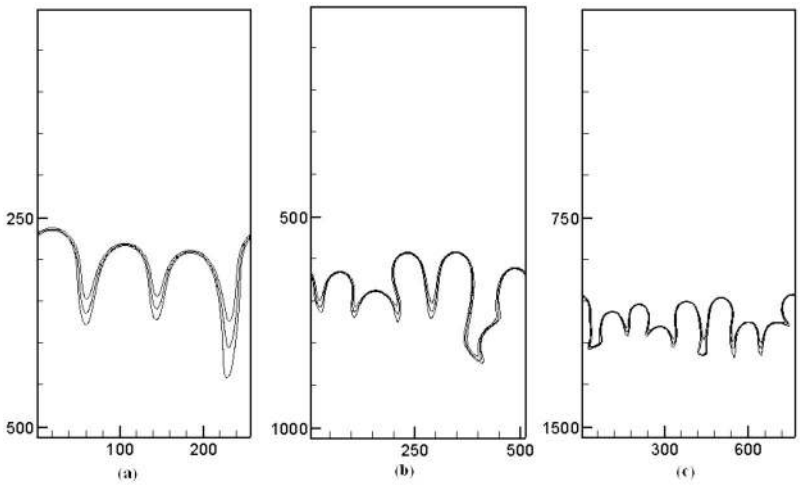

FIG. 10. Nonlinear simulation results showing the concentration contours (0.1–0.3) illustrating the effect of Ra for R=1, Da=0.01, d=0.1, and t=400 s. (a) Ra=256, (b) Ra=512, and (c) Ra=768.

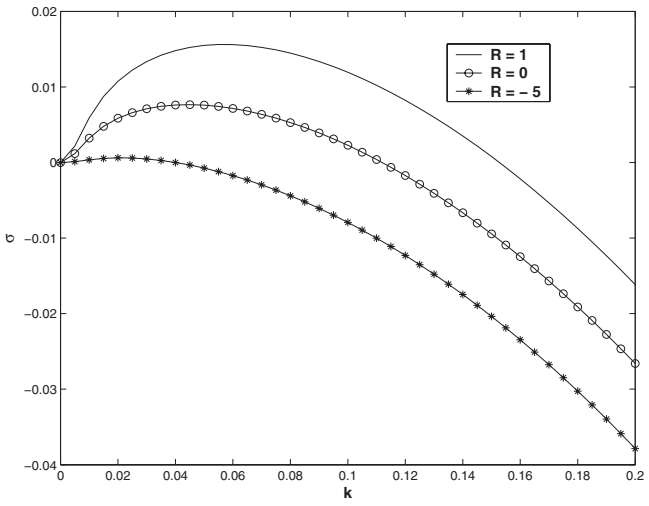

FIG. 11. Dispersion curve showing the variation of growth constant on wave number when heavier products are introduced at the top of the chamber for different mobility ratios with Da=0.01 and d=0.1.

face the number of fingers is more when R=0. The amplitude of the disturbance, however, is more for R=1 as both density and viscosity have a destabilizing effect. They increase the amplitude of the disturbance by acting in tandem. These results from the nonlinear simulations confirm the predictions from the linear stability analysis [Fig. 5(b)].

Figure 10 shows the contour plots of concentration for three different Rayleigh numbers. An increase in Ra physically implies that the system becomes larger. The dimensionless width of the system as well as length of the system is increased proportionately here (because the aspect ratio A is constant). More fingers are observed for larger Ra. Thus, if we examine Fig. 10(b) we see that the number of fingers is almost double that in Fig. 10(a). The wavelength of the spatial structures observed is independent of Ra for R=1.

So far, we have analyzed the system for the case where the products are injected at the bottom to initiate the reaction. The system is gravitationally unstable when the lighter products invade the heavier reactants. This can be stabilized only for $R<0$ (if the products are more viscous than the reactants). Since in general a more dense liquid has a higher viscosity, stabilization of an unstable system would be difficult to attain for the case of injection of the products at the bottom. We now consider the situation where the product is introduced at the top to initiate the reaction.

We consider the gravitationally unstable situation where the product density is higher than the reactant density. The traveling wave generated now moves along the positive x axis. Hence, v in Eq. (21) is replaced by $-v$ for the present case.

The resulting equations, which determine the linear stability, are modified to

$$\frac{d^2\bar{u}}{dz^2} + \frac{1}{\mu_{ss}}\frac{d\mu_{ss}}{dz}\frac{d\bar{u}}{dz} - k^2\bar{u} + \frac{k^2}{\mu_{ss}}\bar{c} = 0, \tag{23}$$

$$\frac{d^2\bar{c}}{dz^2} - k^2\bar{c} + v\frac{d\bar{c}}{dz} - \bar{u}\frac{dc_{ss}}{dz} - Da\frac{\partial f}{\partial c}\bar{c} = \sigma\bar{c}. \tag{24}$$

Now, when the product density is higher than the reactant density, we have a gravitationally unstable situation and hence a fingered interface is observed. The results of the linear stability analysis are shown in the form of dispersion curves in Fig. 11. Here we show these curves for three different values of the parameter R. For R=0, the dispersion curve lies partially above the x axis, and this confirms the gravitational instability of the system. For $R>0$, a heavier less viscous fluid invades a lighter more viscous fluid. This amplifies the disturbance and this is reflected in the dispersion curve moving upward. We observe that for R=−5, the dispersion curve is completely below the x axis and hence the gravitationally unstable system is stabilized. The change in direction is incorporated in the nonlinear simulations by changing the characteristic velocity from U to $-U$. Figure 12 depicts the results of nonlinear simulations when the product is injected at the top. For R=1, both viscosity and density tend to destabilize the interface (the products on top are heavier and less viscous). The fingers observed are distinct. When R=0, only gravity induces instability and this results in the fingers being less prominent as compared to the case R=1. For R=−5, the heavier product is more viscous than the lighter reactant. The higher viscosity of the product is a stabilizing influence, while the higher density of the product is a destabilizing influence. Here, the former dominates over

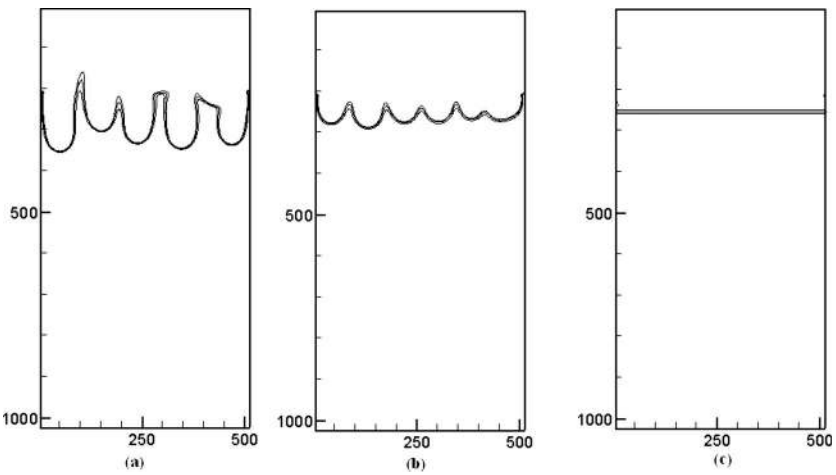

FIG. 12. Nonlinear simulation results showing the concentration contours (0.1–0.3), the effect of viscosity dependent on concentration on density instability when heavier products introduced at the top. The parameters were maintained at Ra=512, Da=0.01, d=0.1, and t=400 s. (a) R=1, (b) R=0, and (c) R=−5.

the latter and the interface of the system remains flat, as can be seen in Fig. 12(c). The results from the nonlinear simulations of Fig. 12 validate the predictions of the linear stability of Fig. 11.

VI. SUMMARY AND CONCLUSIONS

In this work we have analyzed the stability of the interface in miscible displacement in a vertical column. The column is filled with a reactant fluid and we introduce products to initiate an autocatalytic reaction at one end. The interface, i.e., the reaction front, moves up, as the reaction proceeds, in the form of a traveling wave.

We have analyzed the system when both viscosity and density of the fluid vary with concentration. We show that when the system exhibits a density induced instability viscosity dependency of the fluids on concentration can have a stabilizing effect or can amplify the destabilizing effect. When the front travels upward, and the density of the product is lower than that of the reactant, the system is gravitationally unstable. In this case we have shown that when the viscosity of the product is larger than that of the reactant the interface can be stabilized. However, when the product viscosity is lower than the reactant viscosity, the disturbance gets amplified further. The role of the effect of viscosity on stability was found to be independent of the direction of the traveling wave. The effect of kinetic parameters Da and d on the dispersion curve were found to be similar to the case where viscosity was assumed a constant.

[1] S. Hill, "Channeling in packed columns," Chem. Eng. Sci. **1**, 247 (1952).
[2] D. W. Peaceman and H. H. Rachford, "Numerical calculation of multidimensional miscible displacement," SPE J. **2**, 327 (1962).
[3] M. A. Christie and D. J. Bond, "Detailed simulation of unstable processes in miscible flooding," SPE Reservoir Eng. **1**, 514 (1987).
[4] C. T. Tan and G. M. Homsy, "Simulation of nonlinear viscous fingering in miscible displacement," Phys. Fluids **31**, 1330 (1988).
[5] C. T. Tan and G. M. Homsy, "Stability of miscible displacements in porous media: Rectilinear flow," Phys. Fluids **29**, 3549 (1986).
[6] G. M. Homsy, "Viscous fingering in porous media," Annu. Rev. Fluid Mech. **19**, 271 (1987).
[7] A. De Wit and G. M. Homsy, "Viscous fingering in reaction-diffusion systems," J. Chem. Phys. **110**, 8663 (1999).
[8] A. De Wit and G. M. Homsy, "Nonlinear interactions of chemical reactions and viscous fingering in porous media," Phys. Fluids **11**, 949 (1999).
[9] I. Epstein and J. Pojman, *An Introduction to Nonlinear Chemical Dynamics* (Oxford University Press, Oxford, 1998).
[10] M. Böckmann and S. C. Müller, "Coarsening in the buoyancy-driven instability of a reaction diffusion front," Phys. Rev. E **70**, 046302 (2004).
[11] M. Böckmann and S. C. Müller, "Growth rates of the buoyancy-driven instability of an autocatalytic reaction front in a narrow cell," Phys. Rev. Lett. **85**, 2506 (2000).
[12] M. R. Carey, S. W. Morris, and P. Kolodner, "Convective fingering of an autocatalytic reaction front," Phys. Rev. E **53**, 6012 (1996).
[13] D. A. Vasquez, J. W. Wilder, and B. F. Edwards, "Hydrodynamic instability of chemical waves," J. Chem. Phys. **98**, 2138 (1993).
[14] R. Demuth and E. Meiburg, "Chemical fronts in Hele-Shaw cells: Linear stability analysis based on the three-dimensional stokes equations." Phys. Fluids **15**, 597 (2003).
[15] J. Huang, D. A. Vasquez, B. F. Edwards, and P. Kolodner, "Onset of convection for autocatalytic reaction fronts in a vertical slab," Phys. Rev. E **48**, 4378 (1993).
[16] A. De Wit, "Fingering of chemical fronts in porous media," Phys. Rev. Lett. **87**, 054502 (2001).
[17] D. Vasquez, J. Wilder, and B. Edwards, "Wave propagation in Hele-Shaw cells and porous media," J. Chem. Phys. **104**, 9926 (1996).
[18] J. Martin, N. Rakotomalala, D. Salin, and M. Böckmann, "Buoyancy driven instability of an autocatalytic reaction front in a Hele-Shaw cell," Phys. Rev. E **65**, 051605 (2002).
[19] J. Zhu, "A numerical study of chemical front propagation in a Hele-Shaw flow under buoyancy effects," Phys. Fluids **10**, 775 (1998).
[20] B. F. Edwards, J. W. Wilder, and K. Showalter, "Onset of convection for autocatalytic reaction fronts: Laterally unbounded system," Phys. Rev. A **43**, 749 (1991).
[21] J. D. Murray, *Mathematical Biology* (Springer, Berlin, 1989).
[22] A. Saul and K. Showalter, *Oscillations and Traveling Waves in Chemical Systems* (Wiley, New York, 1985).
[23] J. Yang, A. D'Onofrio, S. Kalliadasis, and A. DeWit, "Rayleigh–Taylor instability of reaction-diffusion acidity fronts," J. Chem. Phys. **117**, 9395 (2002).
[24] B. McCaughney, J. A. Pojman, C. Simmons, and V. A. Volpert, "The effect of convection on a propagating front with a liquid product: Comparison of theory and experiments," Chaos **8**, 520 (1998).
[25] J. A. Pojman, V. M. Ilyashenko, and A. M. Khan, "Free-radical frontal plymerization: self-propogating thermal reaction waves," J. Chem. Soc., Faraday Trans. **92**, 2824 (1996).
[26] J. A. Pojman, W. W. West, and J. Simmons, "Propagating fronts of polymerization in the physical chemistry laboratory," J. Chem. Educ. **74**, 727 (1997).
[27] P. M. Goldfeder, V. A. Volpert, V. M. Ilyashenko, A. M. Khan, J. A. Pojman, and S. E. Solovyov, "Mathematical modeling of free-radical polymerization fronts," J. Phys. Chem. B **101**, 3474 (1997).
[28] S. Kalliadasis, J. Yang, and A. De Wit, "Fingering instabilities of exothermic reaction-diffusion fronts," Phys. Fluids **16**, 1395 (2004).
[29] T. Bansagi, Jr., D. Horvath, A. Toth, J. Yang, S. Kalliadasis, and A. De Wit, "Density fingering of an exothermic autocatalytic reaction," Phys. Rev. E **68**, 055301(R) (2003).
[30] J. D'Hernoncourt, S. Kalliadasis, and A. De Wit, "Fingering of exothermic reaction-diffusion fronts in Hele-Shaw cells with conducting walls," J. Chem. Phys. **123**, 234503 (2005).
[31] A. De Wit, "Miscible density fingering of chemical fronts in porous media: Nonlinear simulations," Phys. Fluids **16**, 163 (2004).
[32] A. De Wit, P. De Kepper, K. Benyaich, G. Dewel, and P. Borckmans, "Hydrodynamical instability of spatially extended bistable chemical systems," Chem. Eng. Sci. **58**, 4823 (2003).
[33] J. Fernandez, P. Kurowski, P. Petitjeans, and E. Meiburg, "Density-driven unstable flows of miscible fluids in a Hele-Shaw cell," J. Fluid Mech. **451**, 239 (2002).
[34] F. Graf, E. Meiburg, and C. Härtel, "Density-driven instabilities of miscible fluids in a Hele-Shaw cell: Linear stability analysis of the three dimensional stokes equation," J. Fluid Mech. **451**, 261 (2002).